A PRELIMINARY DESIGN METHOD FOR CORRUGATED LOUVER FIN AND RECTANGULAR OFFSET STRIP FIN HEAT EXCHANGERS

P. Bachmann*, V. Gümmer*, P. Polte§

* Technical University of Munich, Chair of Turbomachinery and Flight Propulsion, Boltzmannstr. 15, 85748 Garching, Germany

§ MTU Aero Engines AG, Dachauer Str. 665, 80995 Munich, Germany

Abstract

With the ongoing climate change and the research in the field of hybrid- and fully-electric aircraft engines, the interest in high-performing cooling systems for these engines rises. The main part of all cooling systems is the heat exchangers. For the design of those aero engines, the influences of the heat exchangers on the performance, aerodynamics, weight, installation space, and other disciplines must be included from the beginning.

This paper's main goal is to define a preliminary design process for a heat exchanger suitable for application in aero engines. A sizing or a rating approach shall be available to either calculate the total dimensions or the total heat transfer of the designed heat exchanger. Moreover, the design process shall be simplified for the user to apply and asses.

A Corrugated Louver Fin and Rectangular Offset Strip Fin heat exchanger are chosen for this work. For the definition of the heat exchanger geometry, non-dimensional design parameters are derived. Correlations from experimental data are used to calculate the Colburn and Fanning friction factor. Specific properties relative to the volume of the heat exchanger are calculated right after the geometric definition. These design properties are used for an early assessment. The properties describe the heat transfer, pressure loss, and mass relative to the volume to asses for the specific application in aero engines.

The dependencies of the design method are the geometry, the flow arrangement, the operating conditions, and the total dimensions, respectively, the total heat transfer. A sensitivity study is done to work out the influences of each design parameter on the design properties of the heat exchangers. Moreover, a recommended process for a specific design parameter choice is given. The scope of the design properties of each heat exchanger type is then compared. For the Corrugated Louver Fin heat exchanger, higher heat transfer and, at the same time, lower pressure loss and mass per volume ratios are possible.

After an introduction, the design parameters are explained and derived in one chapter. In the following chapter, the whole design method is described. In chapter 4, the design parameters and design properties are investigated and the heat exchanger types are compared. In the end, a conclusion follows.

Keywords

heat exchanger; preliminary design method; Corrugated Louver Fin; Rectangular Offset Strip Fin

NOMENCLATURE

Abbreviations

AR	Aspect Ratio
CAR	critical Aspect Ratio
CHF	Channel Height Fraction
CLF	Corrugated Louver Fin
FF	Fin Factor
FOF	Fin Offset Factor
LAF	Louver Angle Factor
LEF	Length Factor
LPF	Louver Pitch Factor
$ROSF$	Rectangular Offset Strip Fin

Greek Symbols

β	compactness or surface area density	
δ	fin thickness	m
η	efficiency	
η_0	extended surface efficiency	
μ	fluid dynamic viscosity	$\mathrm{kgm^{-1}s^{-1}}$
ρ	mean fluid density	$\mathrm{kgm^{-3}}$
ρ_{mat}	material density	$\mathrm{kgm^{-3}}$

doi: 10.25967/570189

τ	fluid shear stress	$\mathrm{kgm^{-1}s^{-2}}$
θ	louver angle	$^\circ$
ε	heat transfer effectiveness	

Indices

0	free flow
air	air
c	cold side
$cell$	cell
$core$	core
f	fin
$flow$	flow cross section
h	hot side
he	complete heat exchanger
i	inlet
l_p	based on louver pitch
max	maximum
min	minimum
n	for every fluid stream
o	outlet
p	passage
$prim$	primary heat transfer
ref	reference
$tubes$	tubes
w	wall
$water$	water

Latin Symbols

$\dot{C}$	heat capacity rate	$\mathrm{Js^{-1}K^{-1}}$
$\dot{m}$	mass flow	$\mathrm{kgs^{-1}}$
$\dot{Q}$	heat transfer rate	W
Nu	Nusselt number	
Pr	Prandtl number	
Re	Reynolds number (based on D_h)	
A	heat transfer surface area	$\mathrm{m^2}$
a	plate thickness	m
b_1	fin height	m
b_2	channel height	m
C^*	minimum to maximum heat capacity rate ratio	
c_p	specific heat of fluid at constant pressure	$\mathrm{Jkg^{-1}}$
D_h	hydraulic diameter	m
E	fluid pumping power per unit surface area	$\mathrm{Wm^{-2}}$
f	Fanning friction factor	
h'	fin edge height	m
H	height	m
h	heat transfer coefficient	$\mathrm{Jkg^{-1}}$
H_t	plate and channel height	m
j	Colburn factor	
k	thermal conductivity	$\mathrm{Wm^{-1}K^{-1}}$
L_f	heat exchanger length	m
l_l	louver length	m
l_p	louver pitch	m
l_s	fin length	m
ml	fin parameter	
N	amount	
NTU	number of transfer units	
p	static pressure	$\mathrm{kgm^{-1}s^{-2}}$
p_f	fin width	m
p_t	passage height	m
s	fin edge width	m
T	static temperature	K
U	overall heat transfer coefficient	$\mathrm{Wm^{-2}K^{-1}}$
u	mean fluid velocity	$\mathrm{ms^{-1}}$
V	volume	$\mathrm{m^3}$
W	width	m
W_t	tube length	m

1. INTRODUCTION

In the field of flight propulsion, heat exchangers are used not only for inter-cooling in combustion aero engines but also for cooling systems, such as electric systems of novel hybrid and all-electric aircraft engines. Heat exchangers that generate high overall heat transfer and low-pressure losses can increase the energy efficiency of cooling systems and thus could reduce the propulsion system's size and weight.

Every design process begins with a preliminary phase. In this phase, simplified calculations balance the requirements for the different disciplines

and define the first draft. Extensive geometric parametrization and precise predictions at the preliminary design phase can lead to a time reduction in the overall design phase. Not only working hours can be saved, but the design quality can also increase.

To calculate the heat transfer through complex surface geometries, extensive numerical methods are usually required. On the other hand, simplified equations often don't consider the dependencies of every aspect of the complex geometry. The method of construction is decisive in the design of heat exchangers. For applications where high heat transfer in a small installation space is needed, heat exchangers with extended heat transfer surfaces (fins) are often used (extended surface heat exchangers), such as plate-fin heat exchangers. Fins can increase the total area by five to twelve times the primary surface area ([1] p. 36-37). In addition, advanced fin features such as louvers or strip fins interrupt the flow, and can increase the heat transfer coefficient two to four times more than the plain fins ([1] p. 36-37). Fin heat exchangers with a high fin density are called compact fin heat exchangers ([2] p. 19-24). These heat exchangers are used in aircraft engines and in the automotive sector, for example.

MTU Aero Engines AG, whose cooperation with this work was created, is investigating fully-electric and hybrid-electric propulsion systems that use compact fin heat exchangers in their cooling systems.

This work analyzes the design of two compact fin heat exchangers: The Corrugated Louver Fin (*CLF*) and the Rectangular Offset Strip Fin (*ROSF*) heat exchanger. Both are two-fluid, direct-transfer type, single-pass, single-phase, crossflow heat exchangers with flat tubes and a fin matrix on the other fluid side. The flat tubes are meant for liquid fluids with high thermal conductivity and density. The fin matrix with the extended heat transfer areas is intended for gases to compensate for the lower thermal conductivity and density. For the liquid side, the higher thermal resistance of the fins would eliminate the advantages of extended surfaces. Fins are recommended for a compact heat exchanger with two gas flow sides.([2] p. 19-24)

The *CLF* heat exchanger is commonly used in the automotive industry and is suitable for low-cost mass production ([1] p. 516-517). Despite the expected higher pressure drop with higher heat transfer, it is capable to outperform a *ROSF* heat exchanger in heat transfer while maintaining the same pressure ([1] p. 516-517). It consists of corrugated fins extending over the full flow length between the plates. These fins are fitted with louvers at a certain angle. It makes no difference to the correlation results whether the fin channels have a triangular shape ([3] p. 535, figure 1, Type A) or a rectangular shape ([3] p. 535, figure 1, Type C) since heat exchangers of both types are used for deriving the correlations used for the calculation (see Appendix B). In figure 1 the geometry of the *CLF* matrix is shown.

The *ROSF* heat exchanger is one of the most widely used types in the aircraft industry ([1] p. 516). It is known to have in general the highest heat transfer to pressure drop ratios of all heat exchangers ([1] p. 516). It has fins of rectangular shape. The fins are separated and staggered with a half fin channel length offset along the flow path. In figure 2, the geometry of the *ROSF* matrix is shown.

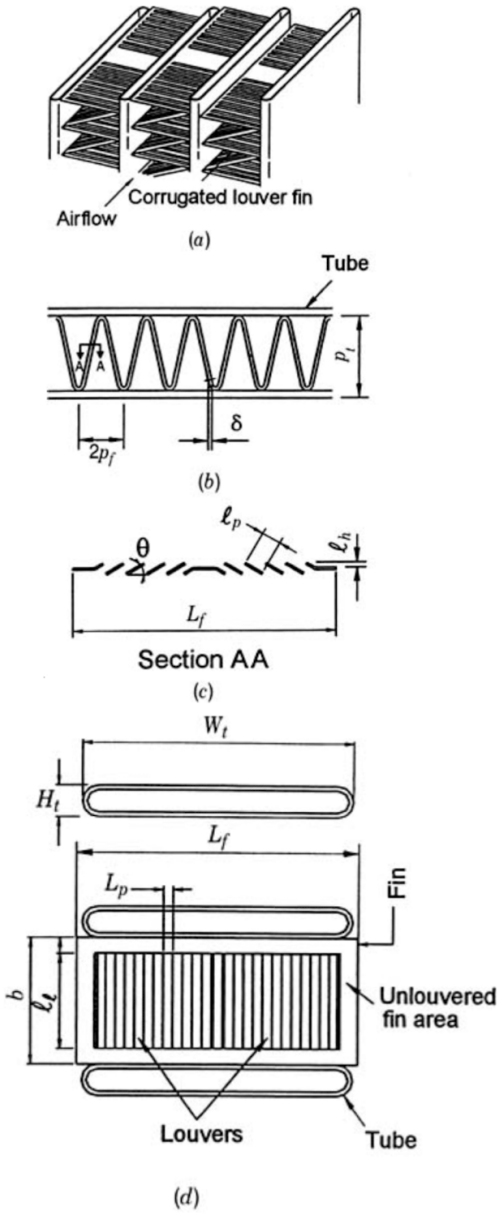

FIG 1. Corrugated Louver Fin matrix ([1] p. 517, figure 7.29)

2. DESIGN PARAMETERS

The design of a heat exchanger is defined by a set of geometric dimensions like the fin thickness or the fin length. They are called geometric parameters. The design here means the specific geometry of an unit cell that makes up the heat exchanger. The number of these cells in the designed heat exchanger is two global dimensions, respectively, calculated later in the process (see Appendix E).

To simplify the design, new dimensionless parameters are introduced, the design parameters.
The following describes the derivation of the geometric parameters from the design parameters. The geometric limits used are the ones from the correlations in Appendix A.
For the *CLF* heat exchanger, nine different geometric parameters define the design (see figure 1): the fin height b_1 (in figure 1 shown as b), the fin width p_f, the louver pitch l_p, the louver angle θ, the louver length l_l, the heat exchanger length L_f, the channel height b_2, the fin thickness δ, and the plate thickness a.
These geometric parameters are entirely defined by the six design parameters:

- AR, FF, LAF, LPF, LEF, CHF

The design parameter Aspect Ratio (AR) is defined as:

$$AR = \frac{b_1}{p_f} \tag{1}$$

The design parameter Fin Factor (FF) has a value between zero and one. It describes the relative size of a fin channel (parameters b_1 and p_f) within the given correlation limits of the correlation (see Appendix A). The larger the factor, the larger the channel. FF always represents the relative value of the allowed size. For example, if $FF = 1$ and AR increases, b_1 eventually reaches its limit. After that p_f is then continuously decreasing to reach the desired AR. The largest absolute value range of b_1 and p_f can be achieved for $AR = CAR$. The Critical Aspect Ration (CAR) is:

$$CAR \approx 5.6 \tag{2}$$

For $AR \geq CAR$ it applies:

$$b_1 = 0.00051 \cdot AR + FF \cdot (0.02 - 0.00051 \cdot AR) \tag{3}$$

$$p_f = \frac{b_1}{AR} \tag{4}$$

For $AR < CAR$ it follows:

$$p_f = \frac{0.00284}{AR} + FF \cdot (0.0036 - \frac{0.00284}{AR}) \tag{5}$$

$$b_1 = p_f \cdot AR \tag{6}$$

The geometric parameter l_l is calculated proportionally to b_1.

$$l_l = \frac{b_1}{1.0811} \tag{7}$$

The Louver Angle Factor (LAF), Louver Pitch Factor (LPF), and Length Factor (LEF) define θ, l_p and L_f within the given correlation limits. These factors have values between zero and one. A single factor was chosen for each of these parameters, as each has an important influence on the design.

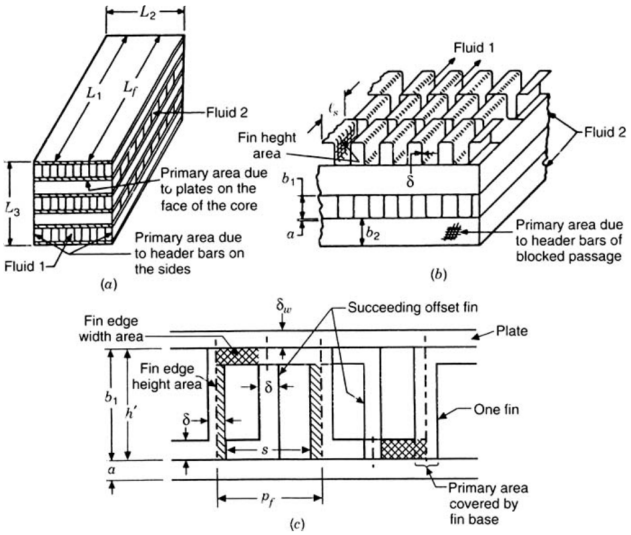

FIG 2. Rectangular Offset Strip Fin matrix ([1] p. 575, figure 8.7b and c)

For LAF and LEF, zero describes the smallest geometric parameter values. The opposite applies to LPF. These boundaries are chosen so that the resulting heat transfer generally increases as LPF and LAF increase. An increasing LEF results in an increased length.

$$\theta = 8.4 + 26.6 \cdot LAF \tag{8}$$

$$l_p = 0.003 - 0.0025 \cdot LPF \tag{9}$$

$$L_f = 0.0156 + 0.0418 \cdot LEF \tag{10}$$

The design parameter Channel Height Fraction (CHF) defines b_2 as a fraction of b_1.

$$b_2 = \frac{b_1}{CHF} \tag{11}$$

Moreover it applies:

$$H_t = b_2 + 2 \cdot a \tag{12}$$

$$p_t = b_1 + H_t \tag{13}$$

Here the geometric parameters δ and a are not considered variables but constants. These thicknesses are mainly dependent on structural aspects, such as the pressure of the fluid flowing through. Generally, the thinner applies, the lower the thermal and aerodynamic resistance.
To simplify the design, the same length is assumed

for the fins and tubes:

$$W_t = L_f \tag{14}$$

For the design of the *ROSF* heat exchanger, six geometric parameters have to be specified (see figure 2): the fin edge width s, the fin edge height h', the fin length l_s, the fin thickness δ, the channel height b_2, the length L_f and the plate thickness. These parameters can be derived from the five design parameters:

- FF, AR, FOF, LEF, CHF

The aim is to keep the design parameters the same as for the *CLF* heat exchanger. However, the new geometry and the different limits require slight changes. The geometric parameter p_f is defined by FF ([1] p. 516):

$$s = \delta \cdot (5.3 + 19.7 \cdot FF) \tag{15}$$

$$p_f = s + \delta \tag{16}$$

b_1 is dependent on p_F and AR ([1] p. 516):

$$h' = AR \cdot (p_f - \delta) \tag{17}$$

$$b_1 = h' + \delta \tag{18}$$

The design parameter Fin Offset Factor (FOF) defines the length of the fin strips. It has a value between zero and one. A high FOF defines many fin offsets, short fin strips and a general high heat transfer.

$$l_s = \delta \cdot (83,3 - 66,6 \cdot FOF) \tag{19}$$

The limits for L_f of the *CLF* heat exchanger are assumed to be realistic limits for general compact heat exchangers and therefore taken for the *ROSF* heat exchanger. L_f is consequently calculated by equation 10. b_2 can be calculated with equation 11. δ and a are considered constants for this heat heat exchanger type as well. Moreover equations 12 and 13 apply here, too.

Even though most of the geometry parameters are limited by the new design parameters, not every combination of these design parameters is possible. There are additional limits due to the used correlations. The user has to take care that these limits are not exceeded. In Appendix A the limits of the design parameters are given.

3. DESIGN METHOD

In the following, the whole calculation process of the design method is explained.

At the beginning of this work's preliminary design method, specific design parameters exist. The following ones must be specified for the *CLF* heat exchanger:

- The Aspect Ratio (AR) of the fin channels
- The Fin Factor (FF) is a quantity for the size of the fin channels
- The Louver Angle Factor (LAF) is a quantity for the size of θ
- The Louver Pitch Factor (LPF) is a quantity for the size of l_p
- The Length Factor (LEF) is a quantity for the size of L_f
- The Channel Height Fraction (CHF) is the fraction of b_2 to b_1

For the *ROSF* the following design parameters must be defined:

- The Aspect Ratio (AR) of the fin channels
- The Fin Factor (FF) is a quantity for the size of the fin channels
- The Fin Offset Factor (FOF) is a quantity for the size of l_s
- The Length Factor (LEF) is a quantity for the size of L_f
- The Channel Height Fraction (CHF) is the fraction of b_2 to b_1

With these values and the calculations of chapter 2 the geometric parameters of the specific heat exchanger can be calculated.

With the geometric parameters, correlations from experimental data can be used to determine each fluid side's Colburn and Fanning Friction factor. The correlations for each heat exchanger type and their calculation are explained in Appendix B. These correlations are chosen because of their dependencies on every geometric aspect, for example, the fin size and even the louver angle for the *CLF*.

Then the surface areas and additional geometric values are calculated. Their belonging calculations are found in Appendix C.

Now the properties (here called design properties) $U \cdot A/V$ and m/V of the heat exchanger and $\Delta p/V$ of its fin matrix are calculated. The calculation process is given in Appendix D. These values can provide a first assessment of the performance of the design. The heat transfer coefficient is the most significant property of a heat exchanger. The mass is also an important property, especially in aviation applications. Moreover, the pressure drop of the fin (air) side is chosen because for cooling systems, often surrounding air or air from the engine is taken, and therefore, the pressure drop is important for the engine performance calculation. All properties are divided by the volume to compare the heat exchangers regarding their installation space which is another significant aspect of flight propulsion. In chapter 4 these values and their dependency on the design parameters are investigated. By selecting a design parameter set, the total length of the heat exchanger L_f is already defined. The other global dimensions, width W_{he} (flow length through the tube) and height H_{he} (increases with the number of tubes) of the heat exchanger, respectively, and the number of unit cells are not determined yet. After the calculations of $U \cdot A/V$ there are now two possible ways to go on. With the specification of the missing total dimensions

of the heat exchanger, the total heat transfer rate of the heat exchanger can be calculated (rating approach: continue with Appendix E.1). In many design applications, the full heat exchanger dimensions are defined by the cross-sectional flow areas and given flow properties calculate these, so also here. So the required additional specifications for this design approach are the inlet temperatures $T_{i,n}$, the specific heat capacities $c_{p,n}$, the mass flows $\dot{m}_n$, the mean densities ρ_n, and the mean velocities u_n of the two fluid streams. Moreover, the desired flow arrangement is defined. If the total dimensions are actually given, continue with equation 63 in Appendix E.1. Figure 3 shows the structure of the whole calculation process for a rating problem. The index "n" means that the inputs are needed for every fluid stream.

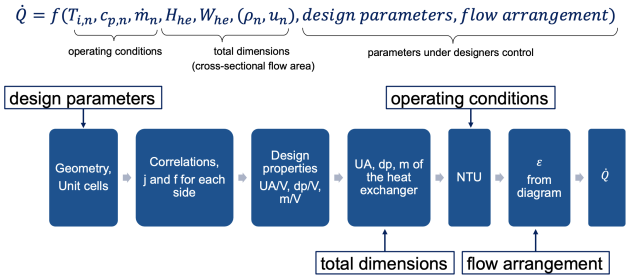

FIG 3. General calculation process for the rating problem

The other option is to define the total heat transfer rate to determine the total dimensions (sizing approach: continue with Appendix E.2). Here, the required additional specifications are the total heat transfer rate $\dot{Q}$, the flow arrangement, the inlet temperatures $T_{i,n}$, the specific heat capacities $c_{p,n}$ and the mass flows $\dot{m}_n$ of the two fluid streams.
In figure 4 the structure of the whole calculation process for a sizing problem is shown.

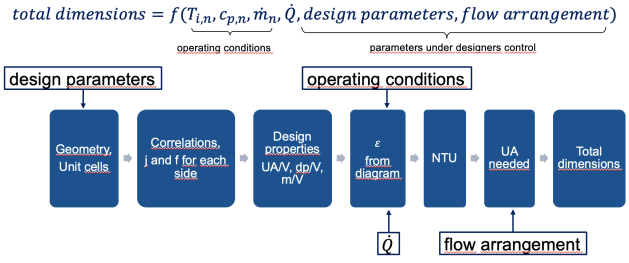

FIG 4. General calculation process for the sizing problem

For a preliminary design, one of these calculation processes is done many times with changing inputs for the design parameter so that iteratively a suitable design is worked out. The design parameters can be changed based on the trends and dependencies discovered in chapter 4.
The so-called cell method can be used (see [4] p.39, chapter 3.1). Here the heat exchanger is divided into a grid of heat exchange calculation cells. After each cell, the temperatures are calculated to approximate the temperature distribution with a higher local discretization.
The preliminary design method of the two heat exchangers can be integrated into automated design loops to design or simulate cooling systems or even entire aircraft engines.
For simulating the influences of the heat exchanger on cooling systems or even complete propulsion systems, the program *NPSS* is used at *MTU Aero Engines AG*.
NPSS stands for *Numerical Propulsion System Simulation* and is an object-oriented, multi-disciplinary design and simulation environment for propulsion systems. It is mainly used for simulating aero engines and was initially developed by *NASA*.([5])

4. RESULTS AND DISCUSSION

4.1. Sensitivity Study

Now trends of the design properties for changing design parameters are discussed. The general qualitative behavior of values of the *CLF* and the *ROSF* heat exchanger are presented. For individual combinations there could be rare exceptions.

- An increase of factor FF leads to a lower $U \cdot A/V$, m/V and $\Delta p/V$ in both heat exchanger types.
- Due to the definition of AR, a variation changes the size of the fin channel, resulting in changing trends. By bringing AR of the *CLF* closer to the CAR the fin channel size increases additionally, and by getting further away, the size decreases and, therefore, $U \cdot A/V$, m/V, and $\Delta p/V$, too. The influence of this size variation on the results equal these of a size variation through FF. For the *ROSF* a decrease of $U \cdot A/V$, m/V, and $\Delta p/V$ is seen with a raise in factor AR
- For the *ROSF* an increase in LEF has the single impact on a lower $U \cdot A/V$. For the *CLF* heat exchanger, $U \cdot A/V$ and m/V increase and $\Delta p/V$ also decrease.
- A higher CHF leads to higher design properties of both types except for the pressure drop of the *CLF*. A decrease is seen here.
- A higher LAF leads to a higher overall heat transfer coefficient and higher pressure loss but doesn't affect the specific heat exchanger density.
- The same applies to LPF. A higher LPF results in a higher $U \cdot A/V$, and $\Delta p/V$. No impact on m/V.
- The FOF decreases the overall heat transfer coefficient and increases the pressure drop. It has no impact on the property m/V.

The Reynolds number range varies for the *CLF* correlation. The correlation depends on Re_{l_p}. Due to the use of the Reynolds number based on D_h (Re), which is more broadly used in literature, the geometry influences the Reynolds number range. The most significant influences on the Reynolds number range are LPF and FF design parameters.

4.2. Recommended Design Parameter Choice

Based on the results of the sensitivity study, a recommended procedure for selecting a suitable combination of design parameters is now presented.
The instructions are intended to choose the highest $U \cdot A/V$ to $\Delta p/V$ ratio for a specific $U \cdot A/V$ value. The property mass is neglected chiefly here. The given limits of the design parameter values and the additional limits to be taken care of by the user are presented in Appendix A.
For the *CLF* heat exchanger, the following selection procedure is recommended:

- Start with a factor of LEF as low as and CHF as high as possible. The values $U \cdot A/V$ increase as well as the $U \cdot A/V$ to $\Delta p/V$ ratio.
- To further increase $U \cdot A/V$, increase LAF and LPF. This comes with a low cost of $U \cdot A/V$ to $\Delta p/V$ ratio.
- To increase $U \cdot A/V$ even further, AR can be increased, and FF decreased. Both come with a high increase in pressure drop. AR should be preferred since it also reduces m/V.

The design parameter choice for the *ROSF* can be made with the following recommended procedure:

- Select the lowest possible FOF and LEF for the highest values of $U \cdot A/V$ and $U \cdot A/V$ to $\Delta p/V$ ratio.
- To further increase the heat transfer, increase CHF and AR. This comes with a low cost of $U \cdot A/V$ to $\Delta p/V$ ratio.
- To increase the heat transfer even further, decrease FF. But with doing so, the pressure loss increases significantly.

4.3. Comparison of the two Heat Exchanger Types

Now the design parameters and their influences on the design properties are investigated. The properties $U \cdot A/V$ and m/V of the whole heat exchanger and $\Delta p/V$ of its fin matrix are investigated. Their values are shown as a function of the Reynolds number of the air (finned matrix) side. This is chosen because the air is often used from inside or outside of the aero engine; therefore, this value is not easy to change in the overall engine design process. So the correct value must be chosen.
Now operating conditions need to be assumed. The values a=0.0006 m and δ=0.000 04 m are considered for both heat exchanger types (*CLF* and *ROSF*). The influence of a variation of these two parameters is not examined. For the finned heat exchanger side, dry air with fixed fluid properties at *International Standard Atmosphere* at 10 km is assumed (k_{fluid}=0.020 07 J s^{-1} m^{-1} K^{-1}; ρ=0.414 kg m^{-3}; μ=1.459 kg m^{-1} s^{-1} ;Pr=0.731 ; c_p=1005 J kg^{-1} K^{-1}. The material of the fins and plates is aluminum with k=239 W m^{-1} and ρ_{mat}=2700 kg m^{-3}. For the tube side of the heat exchanger, water at 20°C with the constant properties Pr=7 , Re=15 000 , d/l=0.001 and k=0.6 W m^{-1} K^{-1} is assumed. The correlation from [4] p. 788, equation 26, 27 for fully developed turbulent flow is used to calculate the flat tubes.

Six different example heat exchangers are created for each heat exchanger type. While selecting the design parameter combinations, care was taken to ensure that all design possibilities were used in order to show the full scope of the resulting values.
The parameters of the individual sample geometries are listed in table 1.

TAB 1. Design parameters for example heat exchangers

	AR	FF	LEF	CHF	LAF	LPF
LouverFin1	8	0.6	0	8	1	0.7
LouverFin2	8	0.8	0	7	0	0
LouverFin3	10	0.4	0.4	7	0.7	0.5
LouverFin4	15	0.3	0	4	1	0.7
LouverFin5	3	0.8	1	2	0	0
LouverFin6	15	0.3	0	3	1	0.7
	AR	FF	LEF	CHF	FOF	
OffsetFin1	5	0.6	0	8	0	
OffsetFin2	6	1	1	3	1	
OffsetFin3	4	0.3	0	8	0	
OffsetFin4	4	0.5	0.5	5	0.5	
OffsetFin5	5	0.3	0	8	1	
OffsetFin6	6	0.8	0	7	0	

Figure 5 shows $U \cdot A/V$ as a function of the Reynolds number. For this and the following figures the values are referenced to the highest data point value (index "ref") of the current figure. A suitable Reynolds number range within the limits of both heat exchanger types is chosen. Nevertheless some graphs don't extent over the entire range. This is caused by the design limits.
The course of the values is strongly increasing at low Reynolds numbers. For higher Reynolds numbers, the values increase slower. It can be seen that very different results can be achieved by changing the design parameters and the heat exchanger type. The figure also shows that only a range of lower values can be reached with the *ROSF* than for *CLF* heat exchangers for the given Reynold number range. "LouverFin4" has the highest values of the *CLF* type and "OffsetFin3" of the *ROSF* type.
In figure 6, the pressure loss of the air side to heat exchanger volume ratio is shown. The pressure loss is raising strongly with increasing Reynold numbers. Here it can be seen that a wide range of values can be achieved with each of the two heat exchanger types. The graphs of the *ROSF* show significantly higher pressure losses than those of the *CLF* heat exchangers.
In figure 7 m/V of the example heat exchangers are compared. The *ROSF* heat exchangers show sig-

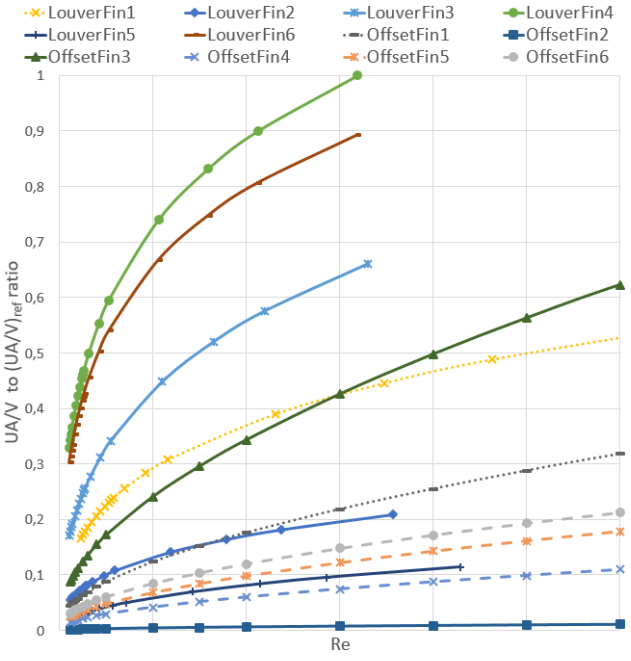

FIG 5. $U \cdot A/V$ **to** $(U \cdot A/V)_{ref}$ **as a function of the Reynolds number of the air side**

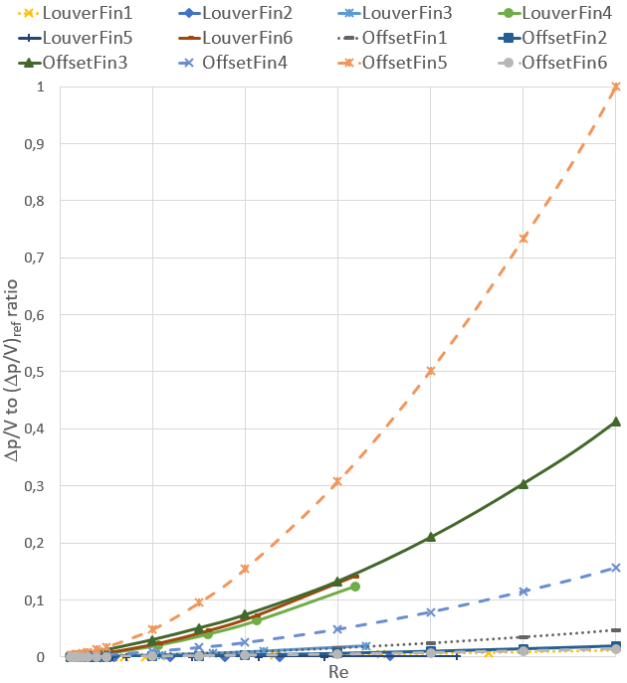

FIG 6. $\Delta p/V$ **to** $(\Delta p/V)_{ref}$ **ratio of the fin matrices of the example heat exchangers as a function of the Reynolds number of the air side**

nificant higher masses. The *CLF* only reach up to around thirty percent of the *ROSF* type with the highest mass. Considering "LouverFin4" in also the previous figures, it has the highest heat transfer values but only the fifth highest pressure loss and the fifth lowest relative mass.
In figure 8 the free flow area to frontal area ratio is shown. Here the *CLF* type shows higher values. This is one of the reasons for the lower relative mass of the *CLF* heat exchangers. A higher free flow area means lower blockage by fin material in the matrix and, therefore, less material. The other factor influencing the mass is the tube size. Looking at figure 9 it is clear that the values of the *CLF* are more than double on average. Since an increase of parameter *CHF* results in an increase of the relative mass, as explained in chapter 4.1, a lower value b_1 is, therefore, also leading to an increased mass. The parameter CHF gives the fraction of b_1 to calculate b_2. Therefore, the decrease of the volume by b_2 is more significant than the decrease in tube mass.
These different limited geometric ranges also affect the other two design properties.
The limits of the design (limits of the design parameters in Appendix A) are defined mainly by the correlations; therefore, the possible value range shown in this chapter is a result of of the limits and not of the construction method of the heat exchanger type. This shows that the two heat exchanger types have different geometric limitations, such as the free flow area and fin height. So a specific comparison between the two different fin matrices with the given properties is not possible.

For a comparison regarding the specific matrix dimensions (compactness) a core volume goodness factor comparison is chosen. The factor $\eta_0 \cdot h \cdot \beta$ describes the heat transfer power per unit temperature difference and unit core volume ([1] p. 707, equation 10.12).
Factor $E \cdot \beta$ describes the friction power expenditure per unit core volume, where E is the fluid pumping power per unit surface area and β the compactness ([1] p. 707, equation 10.13):

$$E \cdot \beta = \beta \cdot \frac{\mu^3}{2 \cdot \rho^2} \cdot \frac{f \cdot \mathrm{Re}^3}{D_h^3} \tag{20}$$

These two factors compare the performance of extended surfaces regarding their unit volume additionally considering a different compactness as well as the hydraulic diameter. Moreover the heat transfer rate, pressure drop, temperature difference between wall and fluid, the fluid flow rate and the fin efficiency are considered.
In figure 10 factor $\eta_0 \cdot h \cdot \beta$ is shown as a function of $E \cdot \beta$. $U \cdot A/V$ and $\Delta p/V$ are shown over same Reynolds number range. The core volume goodness factor here is plotted for the full allowed ranges of the Reynolds number for each heat exchanger. It can be seen that the *CLF* heat exchangers have significantly higher values. Factor $\eta_0 \cdot h \cdot \beta$ is proportional to $1/V$, so for a constant $E \cdot \beta$ higher values indicate higher performance per volume size. ([1] p. 705-708, [6] p. 73-86)

Now, the *CLF* heat exchanger "LouverFin4" and the *ROSF* heat exchanger "OffsetFin3" are choosen for an applied comparison. Both heat exchangers have the highest values of $U \cdot A/V$ and $\eta_0 \cdot h \cdot \beta$ of their types.

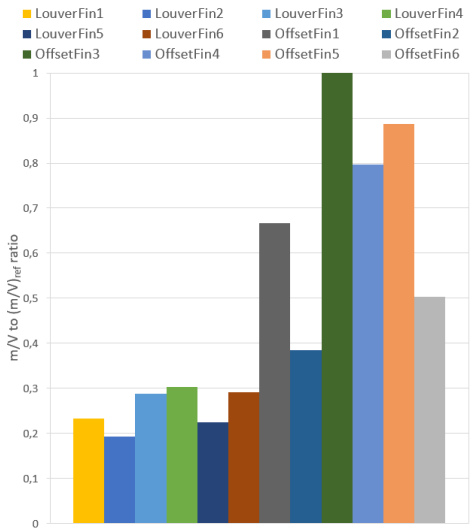

FIG 7. m/V **to** $(m/V)_{ref}$ **ratio of the example heat exchangers**

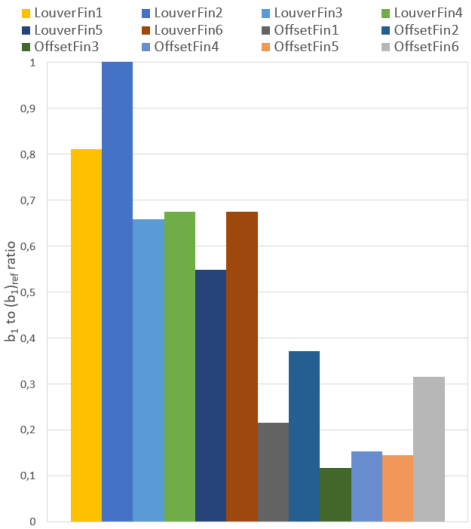

FIG 9. b_1 **to** $(b_1)_{ref}$ **ratio of the example heat exchangers**

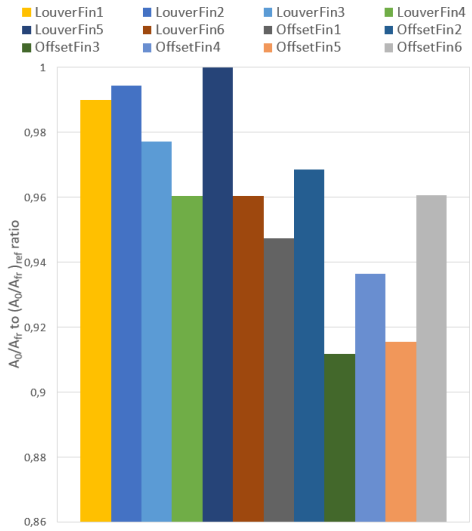

FIG 8. A_0/A_{fr} **to** $(A_0/A_{fr})_{ref}$ **ratio of the example heat exchangers**

Additional assumptions are made: An hot air stream with an massflow of $\dot{m}$=2 kg s^{-1} has a temperatur difference along the heat exchanger of ΔT=22 K. The heat capacity flow ratio is $\dot{C}_{air}/\dot{C}_{water}$=0.9 and the temperatur difference between the inlet flows ΔT_i=30 K. Water has the specific heat capacity ratio c_p=4182 J kg^{-1} K^{-1}.
With these values the sizing approach of the design method (Appendix E.2) is used to calculate the size of each heat exchanger. The result is that "OffsetFin3" has 2.3 times the volume, 7.7 times the mass and 2.7 times the pressure loss of "LouverFin4".

For the here used calculations and their limits, it can be said that the *CLF* heat exchangers have significantly higher heat transfer coefficients, lower pressure drop and less mass per volume for specific Reynolds numbers of the air (finned matrix) side. Also the core volume goodness factor comparison indicates a better performance per volume for the *CLF* heat exchangers. This was confirmed by the results of the sizing of the two leading example heat exchangers.
For the chapter 3 derived preliminary design method and for an application high depended on the volume, the Corrugated Louver Fin heat exchanger is the preferred choice.

5. CONCLUSION

In this work, a new preliminary design method for Corrugated Louver Fin and Rectangular Offset Strip Fin heat exchangers were developed. These two heat exchangers are suitable for the application in aviation because of their compact design and high heat transfer surface areas.
New non-dimensional design parameters were derived in this work which define the heat exchanger geometry. The design parameters simplify the input for the method by their fewer number and by their intuitive use regarding value and influence. Additionally, the design parameters ensure that the geometric parameters stay within the design limits, making the method prone to user errors. Nevertheless, the user can control the most critical parameters individually.
With the given geometry, correlations from experimental data are used to calculate the Colburn and Fanning friction factor based on the geometry. The correlation's advantages are their dependency on every aspect of the heat exchanger and matrix geometry. The dependencies were extended to the geometry, the flow arrangement, the operating conditions, and the total dimensions, respectively, the total heat transfer.
Further, the design properties $U \cdot A/V$, $\Delta p/V$, and m/V can be calculated. With a comparison of these values, an early assessment of the heat exchanger can be made. Thus changes and new iterations can be started quickly.
After that, two design approaches are possible. The rating approach can derive the total heat transfer

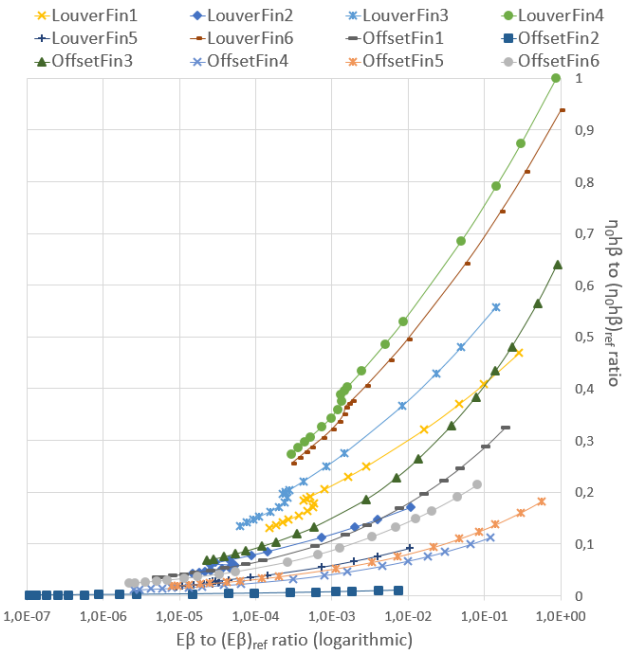

FIG 10. $\eta_0 \cdot h \cdot \beta$ **as a function of** $E \cdot \beta$ **of the example heat exchangers**

from the given total heat exchanger dimensions. The required heat exchanger dimensions can be calculated with the sizing approach and the given total heat transfer.
The influences of the design parameters on the design properties were worked out in a sensitivity study. Moreover, instructions for a recommended design parameters choice were given. At last, the design properties of six example heat exchangers of each type with specific operation conditions were compared. This comparison showed that higher values of $U \cdot A/V$ with at the same time lower values of $\Delta p/V$ and m/V for constant Reynolds numbers are possible with the Corrugated Louver Fin heat exchanger type. Additionally the core volume goodness factors of the example heat exchangers were calculated, which predicted a higher performance per volume for the Corrugated Louver Fin heat exchanger. The size of the heat exchanger with the highest $U \cdot A/V$ and goodness factor values of each type were calculated for an specific operating condition. Here also the heat exchanger of the Corrugated Louver Fin type showed a lower volume, mass and pressure loss.
The Corrugated Louver Fin heat exchanger is the preferred choice for an application such as aviation where installation space plays a decisive role.

Acknoledgements

The authors thank Dr. Reinhold Schaber and Dr. Istvan Bolgar for the support and many valuable discussions.

Contact address:

patrick.bachmann@tum.de

References

[1] R. K. Shah and D. P. Sekulic. *Fundamentals of heat exchanger design*. John Wiley & Sons Inc., New Jersey, 2003.

[2] W. M. Kays, A.L. London, E. Flügel, and A. J. Luther. *Hochleistungswärmeübertrager*. Akademie Verlag, Berlin, 1973.

[3] Y.-J. Chang and C.-C. Wang. A generalized heat transfer correlation for louver fin geometry. *International Journal of Heat and Mass transfer*, 40(3):533–544, 1997.

[4] P. Stephan, S. Kabelac, M. Kind, D. Mewes, K. Schaber, and T. Wetzel. *VDI-Wärmeatlas: Fachlicher Träger VDI-Gesellschaft Verfahrenstechnik und Chemieingenieurwesen*. Springer-Verlag, 2019.

[5] Mechanical Engineering Division Machinery Department Southwest Research Institute. *About Numerical Propulsion System Simulation (NPSS)*. Southwest Research Institute (SwRI), San Antonio, TX, August 2020.

[6] Naef A. A. Qasem and Syed M. Zubair. Compact and microchannel heat exchangers: A comprehensive review of air-side friction factor and heat transfer correlations. *Energy conversion and management*, 173:555–601, 2018.

[7] R. M. Manglik and A. E. Bergles. Heat transfer and pressure drop correlations for the rectangular offset strip fin compact heat exchanger. *Experimental Thermal and Fluid Science*, 10(2):171–180, 1995.

[8] Y.-J. Chang, W.-J. Chang, M.-C. Li, and C.-C. Wang. An amendment of the generalized friction correlation for louver fin geometry. *International Journal of Heat and Mass Transfer*, 49(21-22):4250–4253, 2006.

A. DESIGN LIMITS

There are certain parameter limits to consider if, in Appendix B described, experimental correlations are used.
The limits of the geometric parameters are marked by the maximum and minimum parameter values of all sample heat exchangers taken to derive the correlations. The geometric parameters of the sample *CLF* heat exchangers are found in tables 1 and 2 in [3]. The *ROSF* ones are found in [7] p. 177, table 2.
These parameter limits are used to derive the design parameters.
The design parameters do not restrain the following limits of the parameters. Therefore it has been taken care of by the user that these limits are not exceeded, even after a legitimate choice of design parameters.
For the *CLF* heat exchanger, the additional limits are ([1] p. 517, [3] p. 533, [3] p. 540):

- $0.00082 \leq D_h \leq 0.00502$
- $0.00751 \leq p_t \leq 0.025$
- $0.0015 \leq b_2 \leq 0.005$ (recommended)
- $100 \leq \mathrm{Re}_{l_p} \leq 3000$

The *ROSF* heat exchanger has these additional limits ([7] p. 177, table 2):

- $0.0007 \leq D_h \leq 0.0034$
- $0.14 \leq s/h' \leq 1.04$
- $120 \leq \mathrm{Re} \leq 10000$

B. CALCULATION OF J AND F

With the design parameters selected and the geometric parameters determined, the Colburn factor and the Fanning friction factor can be calculated with the correlations explained in the following.
In [1], experimental data from 91 different heat exchangers from various sources were used for a regressional analysis to calculate a correlation between the Colburn factor (see equation 21) and the Fanning friction factor (see equations 22, 23, and 24) and the geometric parameters for *CLF* heat exchangers. 89.3% of the data used lies within $\pm 15\%$ for the Colburn factor correlation results, and the mean deviation is 7.55% ([3], p. 542-543).
The equation for the Colburn factor is as follows ([3] p. 540, equation 9):

(21)
$$j = \mathrm{Re}_{l_p}^{-0.49} \cdot \left(\frac{\theta}{90}\right)^{0.27} \cdot \left(\frac{p_f}{l_p}\right)^{-0.14} \cdot \left(\frac{b_1}{l_p}\right)^{-0.29} \left(\frac{W_t}{l_p}\right)^{-0.23} \cdot \left(\frac{l_l}{l_p}\right)^{0.68} \cdot \left(\frac{p_t}{l_p}\right)^{-0.28} \cdot \left(\frac{\delta}{l_p}\right)^{-0.05}$$

The correlation for the Fanning friction factor consists of two parts that correlate the factor below and above the Reynolds number $\mathrm{Re}_{l_p} = 150$. Since the course of the Fanning friction factor is discontinuous at this point, the authors have published an extension for the correlation (see [8]). This extension calculates the factor for the range between $\mathrm{Re}_{l_p} = 130$ and $\mathrm{Re}_{l_p} = 230$ and guarantees a smoother transition between the two parts.
So the Fanning friction factor for $\mathrm{Re}_{l_p} < 130$ is calculated by ([8] p. 4250, equations 2, 3, 4 and 1):

(22)
$$\begin{aligned} f_1 &= 14.39 \cdot \mathrm{Re}_{l_p}^{-0.805 \cdot p_f / b_1} \cdot ln\left(1.0 + \left(\frac{p_f}{l_p}\right)\right)^{3.04}, \\ f_2 &= ln\left(\left(\frac{\delta}{p_f}\right)^{0.48} + 0.9\right)^{-1.435} \cdot \left(\frac{D_h}{l_p}\right)^{-3.01} \cdot \\ &\quad ln\left(\left(0.5\mathrm{Re}_{l_p}\right)\right)^{-3.01}, \\ f_3 &= \left(\frac{p_f}{l_l}\right)^{-0.308} \cdot \left(\frac{L_f}{l_l}\right)^{-0.308} \cdot e^{(-0.1167 \cdot p_t / H_t)} \cdot \theta^{0.35}, \\ f &= f_1 \cdot f_2 \cdot f_3 \end{aligned}$$

For $130 \leq \mathrm{Re}_{l_p} \leq 230$ it is calculated by ([8] p. 4252, equations 5 and 6)

(23)
$$f = \left(\frac{\left(1 + 3.6 - 0.02 \cdot \mathrm{Re}_{l_p}\right) \cdot f_{\mathrm{Re}_{l_p}=130}}{2} + \frac{\left(1 - 3.6 + 0.02 \cdot \mathrm{Re}_{l_p}\right) \cdot f_{\mathrm{Re}_{l_p}=230}}{2}\right)^{0.5}$$

and for $\mathrm{Re}_{l_p} > 230$ as follows ([8] p. 4250, equations 2, 3, 4 and 1):

(24)
$$\begin{aligned} f_1 &= 4.97 \cdot \mathrm{Re}_{l_p}^{\left(0.6049 - \frac{1.064}{\theta^{0.2}}\right)} \cdot ln\left(\left(\frac{\delta}{p_f}\right)^{0.5} + 0.9\right)^{-0.527}, \\ f_2 &= \left(\left(\frac{D_h}{l_p}\right) ln\left(0.3 \cdot \mathrm{Re}_{l_p}\right)\right)^{-2.966} \cdot \left(\frac{p_f}{l_l}\right)^{-0.7931 \cdot \frac{p_t}{b_1}}, \\ f_3 &= \left(\frac{p_t}{H_t}\right)^{-0.0446} \cdot ln\left(1.2 + \left(\frac{l_p}{p_f}\right)^{1.4}\right)^{-3.553} \cdot \theta^{-0.477}, \\ f &= f_1 \cdot f_2 \cdot f_3, \end{aligned}$$

In [7] experimental data from 18 different heat exchangers from different sources were used to derive the correlations for the *ROSF* heat exchangers. The Colburn factor is calculated by ([7] p. 177, equation 35):

(25)
$$j = 0.6522 \cdot \mathrm{Re}^{-0.5403} \cdot \left(\frac{s}{h'}\right)^{-0.1541} \cdot \left(\frac{\delta}{l_s}\right)^{0.1499} \cdot \left(\frac{\delta}{s}\right)^{-0.0678} \cdot \left(1 + 5.269 \cdot 10^{-5} \cdot \mathrm{Re}^{1.340} \cdot \left(\frac{s}{h'}\right)^{0.504} \cdot \left(\frac{\delta}{l_s}\right)^{0.456} \cdot \left(\frac{\delta}{s}\right)^{-1.055}\right)^{0.1}$$

The correlation for the Fanning friction factor is as follows ([7] p. 177, equation 34):

(26)
$$f = 9.6243 \cdot \mathrm{Re}^{-0.7422} \cdot \left(\frac{s}{h'}\right)^{-0.1856} \cdot \left(\frac{\delta}{l_s}\right)^{0.3053} \cdot \left(\frac{\delta}{s}\right)^{-0.2659} \cdot \left(1 + 7.669 \cdot 10^{-8} \cdot \mathrm{Re}^{4.429} \cdot \left(\frac{s}{h'}\right)^{0.92} \cdot \left(\frac{\delta}{l_s}\right)^{3.767} \cdot \left(\frac{\delta}{s}\right)^{0.236}\right)^{0.1}$$

The Reynolds number based on l_p is calculated by ([1] p. 517):

(27)
$$\mathrm{Re}_{l_p} = \frac{\rho \cdot u \cdot l_p}{\mu}$$

The Reynolds number based on the hydraulic diameter is defined as follows:

$$\text{Re} = \frac{\rho \cdot u \cdot D_h}{\mu} \tag{28}$$

The hydraulic diameter D_h of the *CLF* matrix is calculated by ([1] p. 580-581, equations 8.76, 8.77, 8.78, 8.79 and 8.82):

$$D_h = 4 \cdot L_f \cdot \left(p_f \cdot b_1 - \delta \cdot \left(\left(b_1^2 + p_f^2\right)^{0.5} - \delta\right)\right) / (2 \cdot W_t \cdot (p_f - \delta) + 2 \cdot p_f \cdot H_t + 2 \cdot L_f \cdot \left(\left(b_1^2 + p_f^2\right)^{0.5} - \delta\right) \tag{29}$$

For the *ROSF* matrix, the hydraulic diameter is calculated by ([7] p. 177, equation 27):

$$D_h = \frac{4 \cdot s \cdot h' \cdot l_s}{2 \cdot (s \cdot l_s + h' \cdot l_s + h' \cdot \delta) + s \cdot \delta} \tag{30}$$

The hydraulic diameter of a flat tube is calculated from the ratio of the cross-sectional area to the circumference of the tube ([1]):

$$D_h = \frac{4 \cdot (b_2 \cdot (L_f - H_t) + \pi \cdot b_2^2/4)}{\pi \cdot b_2 + 2 \cdot (L_f - H_t)} \tag{31}$$

Basic correlations for round pipes can be used for calculating the Fanning friction factor and the Colburn factor of the flat tubes, for example, from [4]. Often correlations calculate the Nusselt number directly. It has to be taken care of that the correlation uses the hydraulic diameter instead of the pipe diameter so that the particularity of the flat geometry of the tube is taken into account.

C. CALCULATION OF SURFACE AREA

Now the heat transfer areas for a heat exchanger unit cell are calculated. The dimensions of a cell (V_{cell}) are defined by equation 51. First, the surface areas of the fins are calculated. The following equation applies to the *CLF* heat exchanger ([1], p. 580, equation 8.77):

$$A_{f,cell} = 2 \cdot L_f \cdot \left(\left(b_1^2 + p_f^2\right)^{0.5} - \delta\right) \tag{32}$$

For the *ROSF* matrix the area is calculated as follows ([1], p. 577, equation 8.71):

$$A_{f,cell} = 2 \cdot h' \cdot l_s + 2 \cdot h' \cdot \delta + s \cdot \delta \tag{33}$$

Then the primary heat transfer area can be calculated. The *CLF* matrix applies ([1], p. 580, equation 8.76):

$$A_{prim,cell} = 2 \cdot W_t \cdot (p_f - \delta) + 2 \cdot p_f \cdot H_t \tag{34}$$

The area for the *ROSF* matrix is calculated as follows ([1], p. 577, equation 8.71):

$$A_{prim,cell} = 2 \cdot s \cdot l_s \tag{35}$$

The total heat transfer area, sometimes referred to as the effective surface area, of a finned matrix cell is calculated as follows ([1], p. 580, equation 8.78, p. 291, equation 4.167):

$$A_{cell} = A_{prim,cell} + \eta_f \cdot A_{f,cell} \tag{36}$$

The total heat transfer surface area of a tube cell is equal to its primary surface area and can be calculated as follows:

$$A_{prim,cell} = p_f \cdot (\pi \cdot b_2 + 2 \cdot (L_f - H_t)) \tag{37}$$

Now the free flow area of a cell is calculated for the *CLF* matrix ([1], p. 580, equation 8.79):

$$A_{0,cell} = p_f \cdot b_1 - \delta \cdot \left((b_1^2 + p_f^2)^{0.5} - \delta\right) \tag{38}$$

For the *ROSF* matrix applies ([1], p. 577, equation 8.72):

$$A_{0,cell} = s \cdot h' \tag{39}$$

The free flow area of a flat tube is now calculated:

$$A_{0,cell} = b_2 \cdot (L_f - H_t) + \pi \cdot \frac{b_2^2}{4} \tag{40}$$

By transferring heat through extended surface areas (fins) and then through the primary surface, the local and average temperature difference between the primary surface and fins and fins and fluid is lower than the difference between the primary surface and fluid in a configuration without fins. This causes a slight reduction in heat transfer. These temperature differences are taken into account by the fin efficiency η_f.([1] p. 258)
For the calculation of the fin efficiency the parameter ml is needed. For the *CLF* fin matrix ml can be calculated as follows ([1], p. 581, equation 8.89):

$$ml = \left(\frac{2 \cdot h}{k_f \cdot \delta} \cdot \left(1 + \frac{\delta}{L_f}\right)\right)^{0.5} \cdot \left(\frac{1}{2} \cdot (b_1^2 + p_f^2)^{0.5} - \delta\right) \tag{41}$$

For the *ROSF* matrix ([1], p. 577, equation 8.75):

$$ml = \left(\frac{2 \cdot h}{k_f \cdot \delta} \cdot \left(1 + \frac{\delta}{l_s}\right)\right)^{0.5} \cdot \left(\frac{b_1}{2} - \delta\right) \tag{42}$$

Assuming thin fins with an adiabatic fin tip, the fin efficiency can be calculated as follows ([1], p. 273, equation 4.134):

$$\eta_f = \frac{tanh(ml)}{ml} \tag{43}$$

The extended surface efficency η_0 is calculated by ([1] p. 289, equation 4.160

$$\eta_0 = 1 - \left(\frac{A_f}{A}\right)(1 - \eta_f) \tag{44}$$

The compactness describes the total amount of heat transfer surface to heat exchanger volume ratio ([1] p. 577 equation 8.70 or p. 581 equation 8.84):

$$\beta = \frac{A_{p,cell} + A_{f,cell}}{V_{cell}} \tag{45}$$

Please note that the compactness is defined differently in some literature.

D. CALCULATION OF THE DESIGN PROPERTIES

The Colburn factor can be transformed into the Nusselt number and finally into the heat transfer coefficient by the following equations ([1], p. 447, equation 7.33 and [1], p. 446, equation 7.26):

$$\mathrm{Nu} = j \cdot \mathrm{Re} \cdot \mathrm{Pr}^{1/3} \tag{46}$$

$$h = \frac{\mathrm{Nu} \cdot k_{fluid}}{D_h} \tag{47}$$

The overall heat transfer coefficient U times the total surface area A of a heat exchanger cell can be calculated. Index "c" describes the cold side, and index "h" the hot side of the heat transfer. The heat resistance of the plate is neglected to simplify the equation ([1] p. 108, equation 3.20):

$$(U \cdot A)_{cell} = \frac{1}{1/(h \cdot A_{cell})_h + 1/(h \cdot A_{cell})_c} \tag{48}$$

With the Fanning friction factor, the pressure loss can be calculated. Since the core pressure loss is the most significant part and the other (entry, exit, and momentum) losses can be neglected, it applies ([1], p. 382 - 389):

$$\Delta p \approx \Delta p_{core} \tag{49}$$

The pressure loss over the cell can thus be approximated (derived from [1], p. 379, equation 6.2):

$$\Delta p_{cell} \approx 2 \cdot f \cdot \rho \cdot u^2 \cdot \frac{L_f}{D_h} = 2 \cdot f \cdot \frac{\mu^2 \cdot \mathrm{Re}^2 \cdot L_f}{\rho \cdot D_h^3} \tag{50}$$

This equation can also be used for the pressure drop calculation of the flat tubes by using the respective values of the tube side and W_{he} instead of L_f.
The volume of a heat exchanger cell is ([1] p. 581, equation 8.83):

$$V_{cell} = p_f \cdot L_f \cdot (b_1 + H_t) \tag{51}$$

The pressure loss and the overall heat transfer coefficient depend on the heat exchanger's volume.

$$\frac{U \cdot A}{V} = (U \cdot A)_{cell} \cdot \frac{1}{V_{cell}} \tag{52}$$

$$\frac{\Delta p}{V} = \Delta p_{cell} \cdot \frac{1}{V_{cell}} \tag{53}$$

The relative mass (m/V) as a measurement of the specific density of the heat exchanger is derived. For the *CLF* geometry applied with $A_{0,cell}$ from equation 38:

$$\begin{aligned} m_{cell} = \rho_{mat} \cdot (W_t \cdot (p_f \cdot b_1 - A_{0,cell}) \\ + p_f \cdot (2 \cdot a \cdot (W_t - H_t) + \pi/4 \cdot (H_t^2 - b_2^2))) \end{aligned} \tag{54}$$

The relative cell mass for the *ROSF* heat exchanger is calculated as follows:

$$\begin{aligned} m_{cell} = \rho_{mat} \cdot (W_t \cdot \delta \cdot (s + b_1) \\ + p_f \cdot (2 \cdot a \cdot (W_t - H_t) + \pi/4 \cdot (H_t^2 - b_2^2))) \end{aligned} \tag{55}$$

Now the relative mass can be calculated:

$$m/V = \frac{m_{cell}}{V_{cell}} \tag{56}$$

A comparison of the values $U \cdot A/V$, $\Delta p/V$ and m/V and their dependence on the design parameters are presented in chapter 4.1.

E. TWO DESIGN APPROACHES

E.1. Rating Approach

The cross-sectional flow areas A_{flow} can be determined by:

$$A_{flow} = \frac{\dot{m}}{\rho \cdot u} \tag{57}$$

The number of tubes, passages, and the number of cells per passage can now be calculated with the free flow area of the cell on each side. For the number of tubes, it applies:

$$N_{tubes} = \left(\frac{A_{cs}}{A_{0,cell}}\right) \tag{58}$$

$$N_p = N_{tubes} - 1 \tag{59}$$

The number of cells per passage of the fin matrix is calculated by:

$$N_{cell,p} = \frac{A_{cs}}{N_p \cdot A_{0,cell}} \tag{60}$$

If the amounts are not a whole numbers, they can be approximated by the nearest integer. Now the total

dimensions of the heat exchanger can be calculated.

(61) $$W_{he} = N_{cell,p} \cdot p_f$$

(62) $$H_{he} = N_p \cdot p_t + H_t$$

The volume of the heat exchanger is determined by:

(63) $$V_{he} = L_f \cdot W_{he} \cdot H_{he}$$

For the overall heat transfer coefficient and the pressure loss of the heat exchanger follows:

(64) $$U \cdot A = \frac{U \cdot A}{V} \cdot V_{he}$$

(65) $$\Delta p = \frac{\Delta p}{V} \cdot V_{he}$$

The $\varepsilon - NTU$ method is used to calculate the heat transfer. The respective heat capacity flow can be calculated for both mass flows $\dot{m}$ ([2] p. 33):

(66) $$\dot{C} = \dot{m} \cdot c_p$$

The smaller heat capacity flow is provided the index "min" and the larger one the index "max". Now the number of transfer units is calculated ([2] p. 36, equation 2-7):

(67) $$NTU = \frac{U \cdot A}{\dot{C}_{min}}$$

For the calculated values of NTU and $C^* = \dot{C}_{min}/\dot{C}_{max}$, a value for the heat transfer effectiveness, can be interpolated from Table 2-14 on [2] p. 78. Figure 11 shows the values of ε as a function of NTU and C^* for a cross-flow heat exchanger with two unmixed fluids, such as the *CLF* or the *ROSF* heat exchanger.
The theoretical maximum amount of heat that can be transferred in a counter-flow heat exchanger with an infinite heat transfer area called $\dot{Q}_{max}$ is now calculated. The flow temperatures at the entries of the heat exchanger are used ([2] p. 38, equation 2-13):

(68) $$\dot{Q}_{max} = \dot{C}_{min} \cdot (T_{h,i} - T_{c,i})$$

The actual total amount of heat transferred by the heat exchanger can now be calculated with ([2] p. 35, equation 2-6):

(69) $$\dot{Q} = \varepsilon \cdot \dot{Q}_{max}$$

The temperatures of the heat exchanger outlets are calculated by ([2] p. 36):

(70) $$T_{h,o} = T_{h,i} - \frac{\dot{Q}}{\dot{C}_h}$$

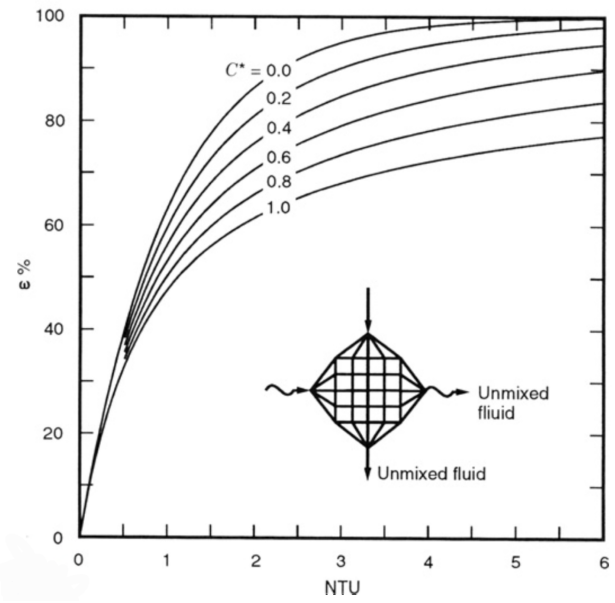

FIG 11. ε as a function of NTU and C^* for a crossflow heat exchanger with two unmixed fluids

(71) $$T_{c,o} = T_{c,i} + \frac{\dot{Q}}{\dot{C}_c}$$

E.2. Sizing Approach

For the second design approach, the calculation from equation 69 to equation 61 (Appendix E.1) can be performed backwards until the dimensions of the heat exchanger are obtained. First, all heat capacity rates and then $\dot{Q}_{max}$ can be calculated. With $\dot{Q}_{max}$ and ε, NTU can be determined. Now the needed $U \cdot A$ can be calculated. With $U \cdot A/V$ the required volume can be derived. With equation 63, a value for H_{he} times W_{he} can be determined. After the calculation of the total dimensions follows the calculation of the cross-sectional areas. With equation 57 the velocities and the densities can be calculated. Then the total pressure loss (with equation 65) can be calculated.